communications materials

ARTICLE

https://doi.org/10.1038/s43246-021-00137-y OPEN

Quantum magnetoconductivity characterization of interface disorder in indium-tin-oxide films on fused silica

David C. Look [1,2]✉, Kevin D. Leedy[2], Marco D. Santia[2,3] & Stefan C. Badescu [2]

Disorder arising from random locations of charged donors and acceptors introduces localization and diffusive motion that can lead to constructive electron interference and positive magnetoconductivity. At very low temperatures, 3D theory predicts that the magnetoconductivity is independent of temperature or material properties, as verified for many combinations of thin-films and substrates. Here, we find that this prediction is apparently violated if the film thickness d is less than about 300 nm. To investigate the origin of this apparent violation, the magnetoconductivity was measured at temperatures $T = 15$ – 150 K in ten, Sn-doped In_2O_3 films with $d = 13$ – 292 nm, grown by pulsed laser deposition on fused silica. We observe a very strong thickness dependence which we explain by introducing a theory that postulates a second source of disorder, namely, non-uniform interface-induced defects whose number decreases exponentially with the interface distance. This theory obeys the 3D limit for the thickest samples and yields a natural figure of merit for interface disorder. It can be applied to any degenerate semiconductor film on any semi-insulating substrate.

[1] Semiconductor Research Center, Wright State University, Dayton, OH, USA. [2] Air Force Research Laboratory Sensors Directorate, 2241 Avionics Circle, Wright-Patterson AFB, OH, USA. [3] National Research Council, 2241 Avionics Circle, Wright-Patterson AFB, OH, USA. ✉email: david.look@wright.edu

Many descriptions and analyses of disorder in metals and highly doped semiconductors have appeared in the literature[1–4], partly because degenerate semiconductor films on semi-insulating substrates are an important part of the electronics industry. Often the substrate has to be transparent to visible light, requiring materials such as sapphire or fused silica (FS). These materials are low cost and stable but can have a serious effect on the electrical properties of the film since, in general, their lattices do not match that of the film. Many of the useful transparent conductive films are oxides, and they include Ga-doped ZnO (GZO), Al-doped ZnO (AZO), and Sn-doped In_2O_3 (ITO)(ref. [5]). In studies of GZO films grown by pulsed laser deposition (PLD), we have found that substrates such as sapphire or FS generate a nonconductive layer ("dead layer") of thickness $\delta d \approx 20$–25 nm in the film next to the interface[6]. Itagaki et al. found a similar-sized dead layer for AZO grown on sapphire by RF sputtering, but they also developed a ZnON buffer layer that led to a greatly reduced δd (ref. [7]). Similarly, for ITO grown on silicon by PLD, Cleary et al.[8] reported a dead layer $\delta d \approx 14$ nm. All of those cases involved thin films mismatched to their substrates, and a common feature was a mobility μ that decreased strongly at low thicknesses, especially for $d \leq 50$ nm. In contrast, the electron concentration n tended to be constant over the whole range $d > \delta d$ as long as it was properly calculated by taking the dead layer into account, i.e., $n = n_{\mathrm{sheet}}/(d - \delta d)$, not n_{sheet}/d (ref. [6]). It was found that the variation of μ with d could often be fitted to an equation $\mu = \mu_0/[1 + d_\mu/(d - \delta d)]$, where the values of d_μ and δd gave a measure of interface quality[6]; in general, however, such an equation had no clear physical basis. In this work, we develop a model based on two, well-defined sources of disorder: (1) the uniform (U) disorder arising from the random arrangement of charged donors and acceptors in any highly doped material; and (2) a nonuniform (NU) disorder generated by the film/substrate interface. As shown below, this model correctly predicts magnetoconductivity over a wide range of film thicknesses, $d = 13$–292 nm, and temperatures, $T = 15$–200 K, and additionally is able to provide a simple, numerical method of characterizing interface quality.

A convenient way to investigate disorder involves magnetoconductivity, defined as $\Delta\sigma(B) = \sigma(B) - \sigma(0)$, where B is the magnetic-field strength. Classical analysis, ignoring the wave nature of the electrons, finds that $\Delta\sigma(B)$ is negative for nondegenerate electrons and vanishes for degenerate electrons. However, quantum analysis of degenerate electrons finds a small positive contribution to $\Delta\sigma(B)$, termed quantum magnetoconductivity (QMC). The QMC arises from electron waves encountering a small fraction of loops in their multiple diffusive scattering paths. Since loops allow traversal in either direction, and each distance is exactly the same, constructive interference can occur at the entry point. This constructive interference increases the probability of loop-type paths, which then decreases the conductivity σ due to the retrograde motion inherent in a loop. The magnitude of this effect is typically about -0.001σ, and is sometimes called "weak localization"[2]. For this process to occur, electron phase must be maintained during the interference event; however, phase can be randomized by a magnetic field or inelastic phonon scattering. A theory of this phenomenon in three dimensions has been developed by Kawabata[4] and yields the following equations:

$$\Delta\sigma(B,T) = \frac{e^2}{2\pi^2\hbar l(B)} \sum_{N=0}^{\infty} 2\left[(N+1+\delta(B,T))^{1/2} - (N+\delta(B,T))^{1/2}\right] - \frac{1}{\left(N+\frac{1}{2}+\delta(B,T)\right)^{1/2}} \quad (1)$$

where

$$\delta(B,T) = \frac{l^2(B)}{4\tau_{\mathrm{ph}}(T)D(T)} = \frac{3e}{4\hbar(3\pi^2 n)^{2/3}\mu_{\mathrm{ph}}(T)\mu_{\mathrm{tot}}(T)B} \quad (2)$$

Here $D(T)$ is the electron diffusion coefficient, τ_{ph} is the inelastic electron–phonon scattering time, and $l(B)$ is a "magnetic length" defined by $l(B) = (\hbar/eB)^{1/2} = 25.656$ nm at $B = 1$ tesla, the field strength used for our measurements. In Eq. 2, we have modified Kawabata's formula by setting $\tau_{\mathrm{ph}} = m^*\mu_{\mathrm{ph}}/e$, and also by invoking the Einstein relation to get $D = (m^*)(v_{\mathrm{f}})^2(\mu_{\mathrm{tot}})/3e$, where v_{f} is the Fermi velocity[9]. It is very important that n and μ_{tot} in Eq. 2 can each be independently determined from the Hall effect, which involves measurements of only current, voltage, and magnetic field[10]. Then, since $\mu_{\mathrm{ph}}(T)$ is the only unknown quantity in Eqs. 1 and 2, its value also is independent of any material parameters.

At very low temperatures, τ_{ph}, and thus also μ_{ph}, will be large since few phonons are present. In such a case, $\delta \ll 1$, and Kawabata's theory[4] gives $\Delta\sigma(B) = 2.908B^{1/2}$ S cm^{-1}, true for any material and independent of temperature. This is a maximum value of $\Delta\sigma$ since $\mu_{\mathrm{ph}}(T)$ will always decrease at higher T because more phonons will be available to scatter electrons. Since $B = 1$ tesla in our experiments, the theory predicts that $\Delta\sigma \leq 2.9$ S cm^{-1}, at any temperature. In earlier studies we verified this prediction in several different degenerate semiconductor materials, e.g., ZnO, GaN, β-Ga_2O_3[9], $ZnGa_2O_4$[11], ScN, In_2O_3, and Si; however, we eventually realized that it seemed to hold only in samples with a thickness of about 300 nm or larger. Indeed, for much thinner films we sometimes have found $\Delta\sigma \gg 2.9$ S cm^{-1}. This fact suggests that the film/substrate interface may be involved, and indeed, as mentioned above, much literature attests to the reduction of measured mobility (μ_{tot}) in very thin films on lattice-mismatched substrates[6–8]. In contrast, for our growth conditions of ITO on FS, given below, we find that μ_{tot} in the thinnest film (13 nm) is only about 20% lower than that in the thickest film (292 nm). On the other hand, $\Delta\sigma$ varies about a factor 10 between these two films. Thus, QMC is a very sensitive and effective way to study and quantify interface disorder.

In this work, we develop a model for $\Delta\sigma$ vs d that quantitatively explains the apparent violation of Kawabata's theory in very thin films. The model is applied to ten ITO films of thickness 13–292 nm and yields three fitting parameters, including $\Delta\sigma_{\mathrm{U}}$, the uniform component of the disorder. In turn, $\Delta\sigma_{\mathrm{U}}$ allows calculation of mobility μ_{ph} due to inelastic phonon scattering, and μ_{ph} can be related to an effective energy of the phonons involved in the scattering.

Results and discussion

Effects of nonuniform disorder on QMC. Kawabata's theory, Eqs. 1 and 2, applies to a degenerate, disordered material in which the disorder is uniform is the sense that the density of charged centers, and thus that of the loops, is constant over the whole volume. We will designate the contribution to $\Delta\sigma$ from these uniformly distributed loops as $\Delta\sigma_{\mathrm{U}}$. However, the interface contribution to disorder, $\Delta\sigma_{\mathrm{NU}}$, is very nonuniform in the direction perpendicular to the interface, and in general will decrease rapidly with distance z from the interface. We postulate that $\Delta\sigma_{\mathrm{NU}}(z) = \Delta\sigma_{\mathrm{NU}}(0)[\exp(-z/\beta)]$ and indeed, such an exponential variation is reasonable and will turn out to fit the data very well. Here, both $\Delta\sigma_{\mathrm{U}}$ and $\Delta\sigma_{\mathrm{NU}}(0)$ are constants that are related to the density of the loops and also to their sizes and orientations with respect to the direction of **B**. We now model the layer as sheets of thickness dz parallel to the interface; thus a sheet at distance z from the interface will have a conductance of $\Delta\sigma(z)dz = \Delta\sigma_{\mathrm{U}}\{1 + [\Delta\sigma_{\mathrm{NU}}(0)/\Delta\sigma_{\mathrm{U}}]\exp(-z/\beta)\}dz$. It is convenient to define $R_{\mathrm{NU}} =$

$\Delta\sigma_{NU}(0)/\Delta\sigma_U$, that is, the ratio of the interface-generated QMC at $z = 0$ to the uniform QMC $\Delta\sigma_U$, which is independent of the interface. Since conductances are additive, the measured conductivity $\Delta\sigma$ will be the integral of $\Delta\sigma(z)dz$ divided by d, giving

$$\Delta\sigma(d) = \frac{1}{d}\int_0^d \Delta\sigma_U\left[1 + R_{NU}\exp(-z/\beta)\right]dz = \Delta\sigma_U\left[1 + \frac{R_{NU}\beta}{d}\left(1 - \exp\left(-\frac{d}{\beta}\right)\right)\right] \quad (3)$$

Below we will determine the parameters $\Delta\sigma_U$, R_{NU}, and β by fitting $\Delta\sigma(d)$ vs d at several different temperatures.

Comparison of our 3D model with an alternative 2D model. Our present model assumes 3D QMC for all the samples, even the 13-nm one. But suppose that 2D QMC is more appropriate for such thin layers, and a change from 3D to 2D accounts for part or all of the observed increase in $\Delta\sigma$ for thinner layers. We must begin our consideration of this question by examining the various "lengths" that might be important in thin-film conductivity analysis. (1) The size of the electron is about $2\pi/k_f(n) \approx 2.46$ nm; (2) the elastic-scattering mean free path may be written as $\lambda_{elas}(n, \mu_{tot}) = (\hbar/e)(3\pi^2 n)^{1/3}\mu_{tot}$, ≈ 6–7 nm, depending on μ_{tot}; (3) the "magnetic length" $= (\hbar/eB)^{1/2} = 25.7$ nm at $B = 1$ tesla. For our samples, these three lengths are not significantly dependent on temperature, and therefore the 13- and 26-nm samples may possibly be expected to have some 2D character. We first note that $k_f\lambda_{elas} \geq 16$ for our samples, and indeed it is required that $k_f\lambda_{elas} \gg 1$ for the validity of a perturbation theory such as Kawabata's. (This relationship should not be confused with the Ioffe-Regel criterion, $k_f\lambda_{elas} = 1$, which applies to the metal-insulator transition point in heavily-doped semiconductors such as ITO[2]. In that case, $k_f\lambda_{elas} \gg 1$ denotes metallic behavior, primarily defined by finite (non-zero) conductivity as $T \to 0$, which indeed holds for our ITO samples, as seen below.) Another length, the inelastic-scattering mean free path, given by $\lambda_{inelas}(n, \mu_{tot}) = (\hbar/e)(3\pi^2 n)^{1/3}(\mu_{tot}\mu_{ph})^{1/2}$, is less than 292 nm for $T > 20$ K, and less than 13 nm at about 200 K. Thus, from these length considerations, we would guess that the 292-nm sample might be 3D-like above 20 K, and most of the other samples, 3D-like above 200 K. However, we can be much more definitive about the 3D nature of the 292-nm sample, as shown below.

To proceed further, we must deal with an established 2D theory, and an obvious choice is that presented by Hikami, Larkin, and Nagaoka (HLN)[12]. This theory is cast in terms of a parameter "$a\tau_\varepsilon$" where $a = 4DeB/\hbar$ and τ_ε represents the dominant form of inelastic scattering, whether electron–electron, electron–phonon, or spin–orbit scattering. For doped semiconductors, with typical concentrations $n \sim 5\times10^{20}$ cm^{-3}, a factor 100× less than that of metals ($n \sim 5\times10^{22}$ cm^{-3}), phonon scattering will be dominant. Indeed, we find that our electron–phonon scattering formula, Eq. 4, well describes the temperature dependence of our QMC data, as shown earlier[9]. We then set $\tau_\varepsilon = \tau_{ph}$, and will for convenience define the

$$\mu_{ph}(T) = \frac{4\pi\varepsilon_0(3/\pi)^{1/3}\hbar^3 n^{1/3} T\sinh^2\left(\frac{T_{ph}}{2T}\right)}{ekT_{ph}^2(m^*)^2(\varepsilon_0/\varepsilon_\infty - 1)} \quad (4)$$

associated mobility as $\mu_{ph} = e\tau_{ph}/m^*$. This term then fits into $\delta(B, T)$, Eq. 2 of the present paper, and gives by far the dominant temperature dependence in $\delta(B,T)$ since n and $\mu_{tot}(T)$ are nearly flat. For comparison with HLN's 2D theory, we consider the very low temperature data, for which $\delta \ll 1$. For our 292-nm sample, $\Delta\sigma(B,T)$, with $B = 1$ tesla in our experiments, is plotted in Fig. 1.

Note that the low-T data, for which $\delta \ll 1$, are very close to Kawabata's prediction, i.e., $\Delta\sigma(\text{low-}T) = 290.8$ S m^{-1}. This number involves no material parameters and is not adjustable in any way. Because $\Delta\sigma$ vs T agrees so closely with 3D theory, we are justified in using Eqs. 1 and 2 to calculate $\mu_{ph}(T)$, representing the inelastic phonon scattering mechanism, as described above. This same scattering mechanism must of course be incorporated in any 2D theory applied to the same sample, including the HLN theory. Fortunately, their parameter "$a\tau_\varepsilon$" can be written in terms of our parameter δ (Eq. 2) as $(a\tau_\varepsilon)^{-1} = (2/3)\delta$. (The "2/3" arises from the change from 3 to 2 dimensions and is unimportant in the subsequent calculations.) HLN give a formula (their Eqn. 19) for $a\tau_\varepsilon \gg 1$ (or $\delta \ll 1$): $\Delta\sigma_{2D} = (e^2/2\pi^2\hbar)\ln(1/\delta)$, where $e^2/2\pi^2\hbar = 1.233\times10^{-5}$ S, the unit of quantum conductance. To convert the units in $\Delta\sigma_{2D}$ from S to S m^{-1}, we divide by 292×10^{-9} m, and the result is plotted in Fig. 1. The fit is not very good and there are no undetermined parameters that could make it better. However, we can go one step further by comparing 2D and 3D for the 13-nm sample, which should give a much better fit to the HLN formula than was found for the 292-nm sample. As shown in the inset of Fig. 1, the 2D fit at 13-nm thickness is not better than that at 292-nm, but actually much worse; therefore, the large increase of $\Delta\sigma$ in thinner samples cannot be attributed to a switch from 3D character in the thicker samples to 2D in the thinnest ones.

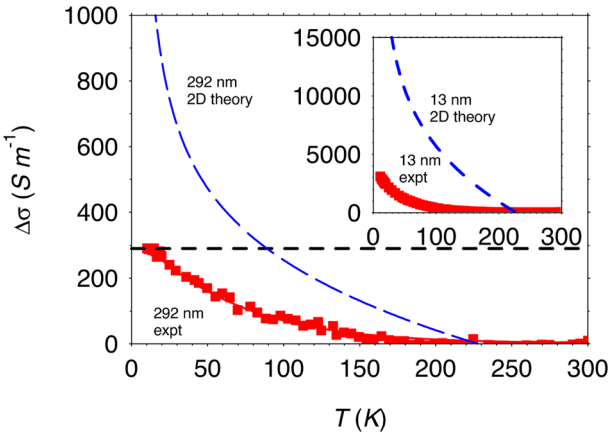

Fig. 1 Temperature dependence of magnetoconductivity. Closed red squares: experimental $\Delta\sigma$ data in units of S m^{-1} for 292- and 13-nm layers. Dashed blue curved lines: predictions of 2D theory, normalized to 292 nm in main plot and 13 nm in inset. Dashed black straight line: $\Delta\sigma = 290.8$ S m^{-1}, the Kawabata 3D prediction at very low T.

Temperature and thickness dependence of mobility and sheet concentration. Figure 2 presents the sheet concentration n_{sq} and mobility μ_{tot} vs thickness d at room temperature for all ten ITO samples. The utility of an n_{sq} vs d plot is to show the variation of the volume concentration n vs d, since n is just the slope of n_{sq} vs d; also, the intercept on the abscissa gives the dead layer thickness, δd. The slope gives $n = 5.65\times10^{20}$ cm^{-3}, nearly constant with thickness down to that of the thinnest layer, only 13 nm. Furthermore, $\delta d < 1$ nm, far lower than, e.g., values found for Ga-doped ZnO on sapphire or on FS[6]. Finally, μ_{tot} is high and also nearly constant at about 38 cm^2 V^{-1} s^{-1}, again unusual for lattice-mismatched growth. Thus, the present set of samples is ideal for this study.

Figure 3 displays temperature dependences of the resistivity $\rho 0$ ($B = 0$), mobility μ_{tot}, and concentration n, for the thickest (292 nm) and thinnest (13 nm) layers. First note that n is constant in both layers, showing good degeneracy, and the values of n differ by only 3% in magnitude. Secondly, $\rho 0$ and μ_{tot} each have about a 20% difference between their respective values in thick and thin layers, although it would normally be much larger in typical lattice-mismatched systems. But the most astonishing difference

involves the values of $\Delta\sigma$, differing by a factor 10 at low temperatures. This huge effect on $\Delta\sigma$ in very thin films is the subject of this study and will be shown to arise from interface disorder.

However, it also reveals that QMC is a very sensitive probe of interface effects, much more so than that of other electrical properties, such as n and μ.

Figure 4 shows plots of $\Delta\sigma$ vs d at temperatures of 15, 30, 50, 80, and 150 K. (Other measurements of $\Delta\sigma$ vs d, not shown to avoid clutter, are at 20, 40, 60, 70, 100, and 130 K). Each curve is fitted to Eq. 3, $\sigma(d) = \Delta\sigma_U\{1 + [R_{NU}\beta/d][1 - \exp(-d/\beta)]\}$, where $\Delta\sigma_U$ represents the uniform disorder arising mainly from the randomness of the donors, and $R_{NU} = \Delta\sigma_{NU}(0)/\Delta\sigma_U$, i.e., the ratio of the nonuniform disorder at $z = 0$ to the uniform disorder, which is constant everywhere. At $B = 1$ tesla, fits of $\Delta\sigma(d)$ vs d at each temperature yield $\Delta\sigma_U$, R_{NU}, and β. It turns out that $\beta = 6.15 \pm 0.6$ nm for all samples, nearly independent of temperature and thickness, while both $\Delta\sigma_U$ and R_{NU} decrease as temperature increases. The temperature independence of β occurs because the spatial distribution of loops is fixed. However, the ability of the loops to affect conductivity, represented by $\Delta\sigma_U$ and $\Delta\sigma_U R_{NU}$, is temperature dependent because the strong inelastic phonon interactions at higher temperatures destroy the constructive electron-wave interference more completely. Besides temperature dependences we must also consider the thickness dependences of $\Delta\sigma_U$ and $\Delta\sigma_{NU}$. At a given temperature, $\Delta\sigma_U$ remains constant as d is increased, but $\Delta\sigma_{NU}$ continuously decreases because of the $[1 - \exp(-d/\beta)]$ term, until at some thickness, designated as d^*, $\Delta\sigma_{NU} < \Delta\sigma_U$. The value of d^* is given by solving $[R_{NU}\beta/d^*][1 - \exp(-d^*/\beta)] = 1$, but for practical purposes, $d^* \approx R_{NU}\beta$. Its significance is that, for $d > d^*$, the surface is far enough away that it is basically unaffected by the interface damage propagating upward. Thus, d^* serves as a useful figure of merit for a layer/substrate interface. It is expected that homoepitaxial layers should have a good interface and thus a small d^*, and we have found this to generally be true. Also, a good buffer layer[7] should make d^* smaller. For $T = 15$, 80, and 150 K, $d^* = 300$, 122, and 76 nm, respectively. A reasonable fit to all of the d^* values up to 150 K gives $d^*(T) \approx [330e^{-T/42} + 63]$ nm. For temperatures much higher than 150 K, e.g., 300 K, the first term is negligible so that $d^* \approx 63$ nm. This rough value of d^* might suffice as a first estimate of the required thickness of ITO on FS to minimize surface disorder for a device operating at room temperature.

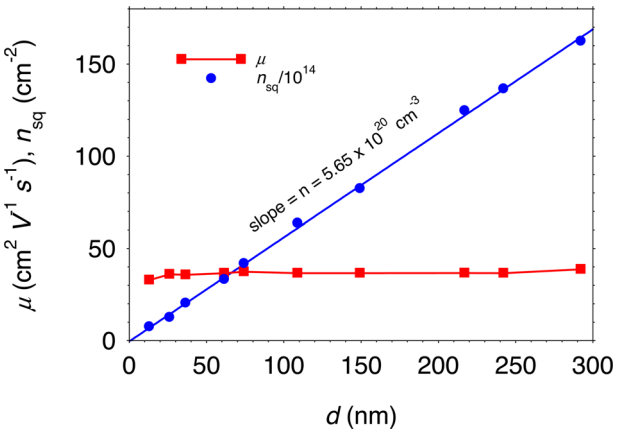

Fig. 2 Sheet carrier concentration and mobility as a function of thickness at room temperature. The slope of sheet carrier concentration n_{sq} (solid blue circles) vs thickness d is the volume carrier concentration n (solid blue line), which is nearly constant at 5.65×10^{20} cm^{-3}. The mobility μ (solid red squares) is about 38 cm^2 V^{-1} s^{-1} and only a weak function of d.

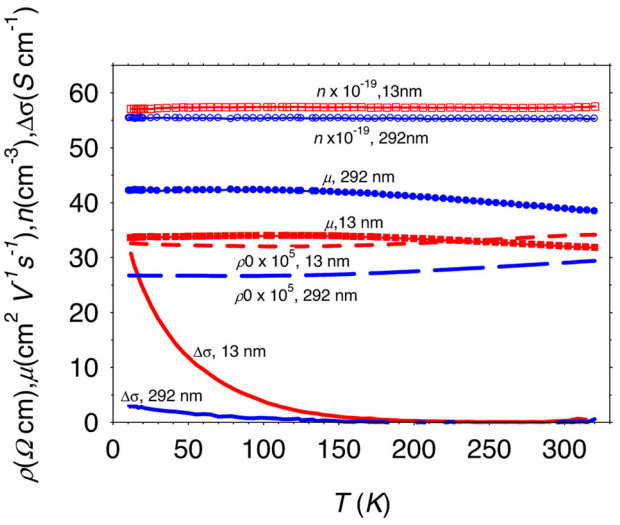

Fig. 3 Temperature dependence of resistivity, volume concentration, mobility, and magnetoconductivity. Carrier concentration n: open red squares, 13 nm sample; open blue circles, 292 nm sample. Mobility μ: closed red squares, 13 nm; closed blue circles, 292 nm. Resistivity, $\rho 0$: dashed red line, 13 nm; dashed blue line, 292 nm. Magnetoconductivity $\Delta\sigma$: red solid line, 13 nm; blue solid line, 292 nm. At low temperatures, $\Delta\sigma$ has by far a stronger thickness dependence than that of n, μ, and $\rho 0$.

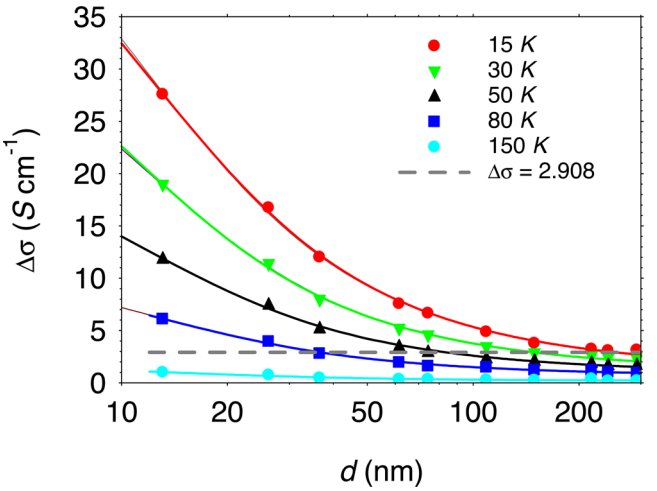

Fig. 4 Magnetoconductivity vs thickness at various temperatures. Solid symbols, experimental values of magnetoconductivity $\Delta\sigma$; solid lines, theoretical fits of symbols to $\Delta\sigma\ (d) = \Delta\sigma_U\{1 + [R_{NU}\beta/d][1 - \exp(-d/\beta)]\}$. Red circles, 15 K; green triangles, 30 K; black triangles, 50 K; dark blue squares, 80 K; light blue circles, 150 K. Dashed line, $\Delta\sigma = 2.908$ S cm^{-1}, which is the theoretical maximum QMC for uniform disorder.

Determination of mobility related to inelastic phonon scattering. To investigate interfaces by QMC, only conductivity measurements are necessary, not Hall-effect measurements. However, to study the phonons responsible for inelastic scattering, represented by μ_{ph}, we must also know n and μ_{tot} (obtained from the Hall effect) so that the only unknown in Eq. 2 is μ_{ph}. It is worth noting that the interface disorder is not expected to greatly affect the phonon spectrum itself, but its nonuniformity can affect our ability to study it via Kawabata's theory, which requires uniformity. In short, only the uniform portion, $\Delta\sigma_U$, is subject to his theory. (In earlier studies[9,11,13] of μ_{ph} in various materials, we

fortunately used very thick samples because, as seen in Eq. 3, the uniform component of disorder $\Delta\sigma_U$ then becomes the dominant term.) From $\Delta\sigma_U$ in the present samples we determine μ_{ph} for $T = 15$–150 K and the results are shown in Fig. 5. For comparison, we also plot μ_{tot} for the 292-nm sample. Clearly, μ_{ph} is strongly temperature dependent, as would be expected, but it does not greatly influence the temperature dependence of μ_{tot}, because $\mu_{ph}^{-1} \ll \mu_{tot}^{-1}$over the whole range. The magnitudes of $\Delta\sigma_U(T)$ at all temperatures are consistent with Kawabata's limit, i.e., $\Delta\sigma(d) \leq 2.9\ \mathrm{S\ cm^{-1}}$, and they also lead to reasonable values of μ_{ph}.

On the other hand, to fully understand μ_{ph} we must include all of the phonons responsible for the electron–phonon scattering. That is a very difficult problem because of the large number (80) of phonon branches in In_2O_3. However, a different approach, introduced earlier[9], is to calculate a single effective phonon energy, $E_{ph}(T) = kT_{ph}(T)$, that produces the required scattering at temperature T. The calculation involves three steps: Step 1, fit $\Delta\sigma(d,T)$ vs d, Eq. 3, to get $\Delta\sigma_U(T)$; Step 2: solve $\Delta\sigma_U(\mu_{ph},T)$ for $\mu_{ph}(T)$ in Eqs. 1 and 2; Step 3: solve $\mu_{ph}(T_{ph},T)$ for T_{ph} in Eq. 4. The results are shown in Fig. 6, and the calculated values of E_{ph} cover an energy range of 7–76 meV over the temperature range 15–150 K. There is no certainty that the E_{ph} vs T curve can be extended beyond 150 K, but if so, we can fit it with $E_{ph} = 137[1 - \exp(-T/172)] - 4.17$, which leads to $E_{ph} = 109$ meV at 300 K.

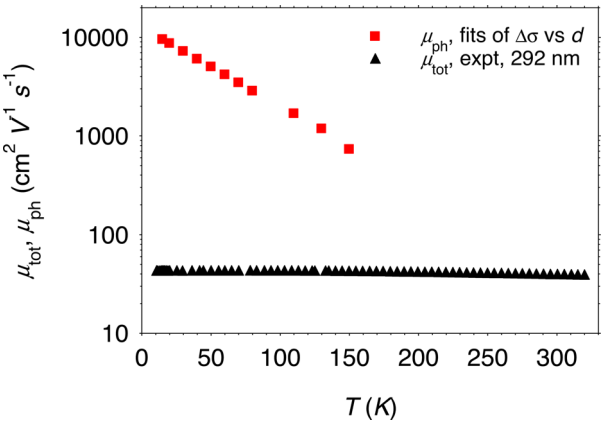

Fig. 5 Temperature dependence of total mobility and phonon-related contribution. Black triangles: total Hall mobility μ_{tot} measured for 292-nm-thick sample. Red squares: calculated mobility μ_{ph} due to inelastic electron–phonon scattering.

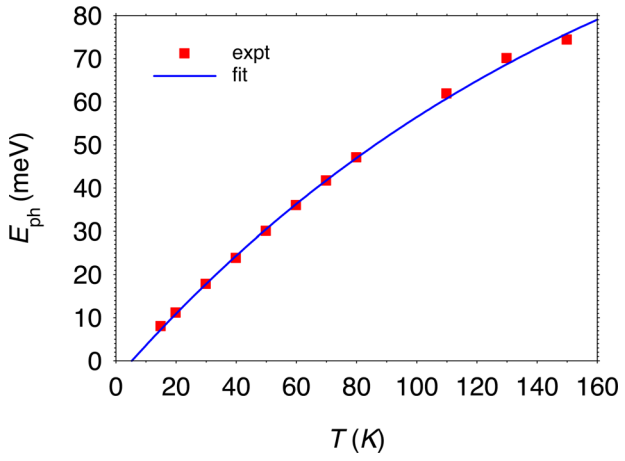

Fig. 6 Temperature dependence of effective phonon energy. Symbols, calculated values of E_{ph} at temperature T. Solid line, fit to $E_{ph}(T) = a[1 - \exp(-T/b)] + c$, where $a = 137$ meV, $b = 172$ K, and $c = -4.17$ meV.

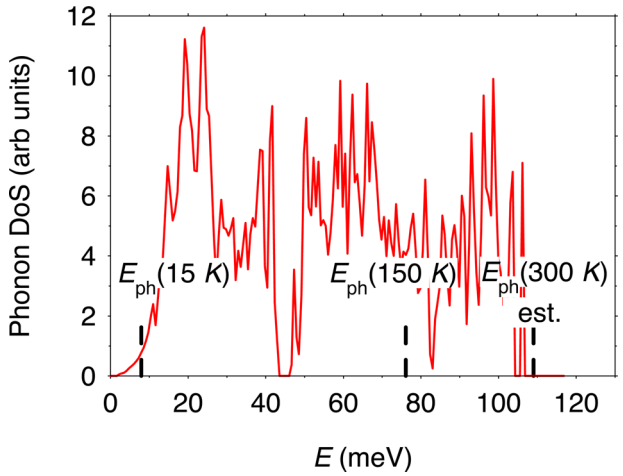

Fig. 7 Theoretical phonon density of states for In_2O_3 and effective phonon energies at 15, 150, and 300 K. Solid red line: phonon density of states (DoS) for perfect-crystal In_2O_3 calculated by density functional theory (DFT). Vertical dashed lines: effective phonon energy E_{ph} calculated from quantum magnetoconductivity (QMC) at temperatures 15 and 150 K, and estimated at 300 K. Note that the ranges of energies determined by DFT and QMC are quite similar.

The reasonableness of these phonon energies can be addressed by investigating their origin, the phonon density of states (DoS), via DFT. For comparison, in a simple semiconductor such as GaN, with two atoms in the unit cell, only one phonon is dominant for scattering electrons at room temperature, a longitudinal optical phonon of energy 93 meV. For more complicated semiconductors, such as Ga_2O_3 with ten atoms in the unit cell, or In_2O_3 with eighty, many phonons take part in the scattering process. Approximate[14] as well as first-principles[15,16] calculations of electron–phonon scattering in Ga_2O_3 have been carried out but only for the perfect crystal, in which symmetry considerations are very important. In a disordered crystal, such as that considered here, symmetries are broken, and the DoS of all phonons, shown in Fig. 7, becomes relevant. Note that the range of the effective phonon energies determined by QMC is very similar to the range of phonon energies calculated by DFT. However, we would expect a broadening and smoothing of the perfect-crystal DoS due to disorder, discussed below.

The lowest energy structures of In_2O_3 are cubic bixbyite, with two atomic arrangements:[17] In_2O_3-I, which has space group No. 199, eight formula units per unit cell, three types of In and two types of O; and In_2O_3-II, which has space group No. 206, eight formula units per unit cell, two types of In and one type of O atoms. In agreement with ref. [17]. our DFT calculations find that these two structures have similar total energies, within 10 meV of each other. In addition, the total energies of In substituted by Sn (Sn_{In}^{+1}) are similar in the two phases for models with one Sn atom per crystallographic cell (80 atoms, i.e., Sn density of $9.76 \times 10^{20}\ \mathrm{cm^{-3}}$) as well as one Sn atom per primitive cell (40 atoms, i.e., Sn density of $1.95 \times 10^{21}\ \mathrm{cm^{-3}}$). We find that the phonon density of states for these model defects has minimal broadening by comparison to that of the pristine material. This can be understood from the small difference between the atomic masses of In and Sn (111.8 a.u. vs 118.7 a.u.) and the small difference between their atomic numbers (49 vs 50), suggesting that Sn has a relatively small effect on the elastic constants. This situation is different from that of degenerately Si-doped β-Ga_2O_3 and $ZnGa_2O_4$, where Si differs significantly from Ga both in mass

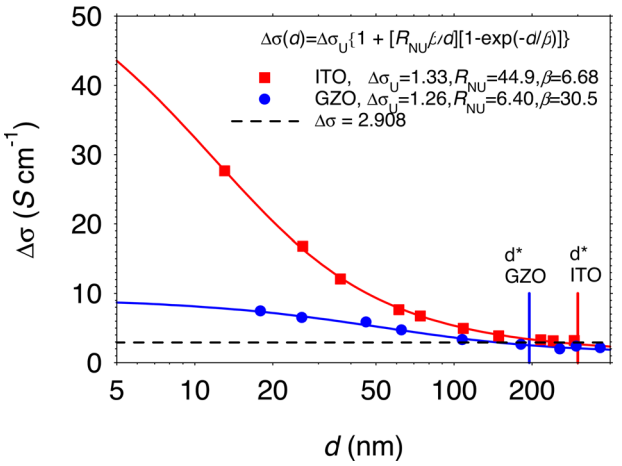

Fig. 8 Thickness dependence of magnetoconductivity in different materials. Comparison of interface quality for different materials, Sn-doped In_2O_3 (ITO) and Ga-doped ZnO (GZO), grown by the same method (pulsed laser deposition) on the same substrate material (fused silica) using the same apparatus. Squares, ITO. Circles, GZO. Solid lines, fits to $\Delta\sigma\,(d) = \Delta\sigma_U\{1 + [R_{NU}\beta/d][1 - \exp(-d/\beta)]\}$. The figure of merit, $d^* = R_{NU}\beta$, is 300 nm for ITO and 195 nm for GZO.

(28.08 a.u. vs 111.8 a.u) and in atomic number (14 vs 49). Therefore we considered additional sources of phonon broadening. A prevalent point defect driven by degenerate doping of In_2O_3 is known to be the oxygen interstitial O_i[17], which acts as a compensating center. We find that the phonon density of O_i^{-2} has a significant broadening especially in the lower part of the spectrum. In addition, we find that the main peaks in the phonon spectra of pristine In_2O_3-I are shifted by a few meV relative to those of In_2O_3-II and have different widths. Given that these two phases are equally likely to form, we expect the resulting spectral function for electron–phonon scattering to be an average of these two densities of states, resulting in additional broadening.

A final requirement of the usefulness of QMC and Eq. 3 is that it be applicable to other degenerate films on other semi-insulating substrates. Although we have only recently begun looking at other layer/substrate systems, previous unrelated programs over a two-year period had involved Ga-doped ZnO (GZO) layers of various thicknesses grown on fused silica in the same PLD system as that used for the present ITO growths. The 15-K QMC results of the GZO samples are plotted in Fig. 8 along with those of the 15-*K* ITO samples shown above in Fig. 4. The fitting parameters of the GZO are $\Delta\sigma_U = 1.26$ S/cm, $R_{NU} = 6.40$, and $\beta = 30.5$ nm, to be compared with those of the ITO, $\Delta\sigma_U = 1.33$ S/cm, $R_{NU} = 44.9$, and $\beta = 6.68$ nm. Interestingly, the differences in R_{NU} and β between ITO and GZO are very large, but the difference in $d^* = R_{NU}\beta$, 195 nm for GZO and 300 nm for ITO, is only a factor 1.5. These results demonstrate that interface damage can propagate far into the film by having either a large initial value (high R_{NU}, as in ITO), or a large decay value (high β, as in GZO). Both are important when considering the best substrate material, or designing an appropriate buffer layer.

Conclusions

We have developed a model to explain an apparent strong violation of Kawabata's 3D theory of quantum-based magnetoconductance in degenerate semiconductors, which states that $\Delta\sigma\,(B) \le 2.908B^{1/2}$ S cm^{-1}, independent of material or temperature. We find that this theory holds well for films of thickness $d = 300$ nm or greater, but not for much thinner films. The Kawabata theory implicitly assumes uniform disorder, $\Delta\sigma_U$, which would be expected from the random locations of large densities of charged donors and acceptors. However, thin films require a substrate for stability and the film/substrate interface can introduce a non-uniform disorder, $\Delta\sigma_{NU}(d)$, into the film. Our model includes both uniform and nonuniform types of disorder and was tested with films of ITO, $d = 13$–192 nm, grown on fused silica by PLD. Electron–phonon scattering theory predicts effective phonon energies E_{ph} of 7 meV at 15 K, and 76 meV at 150 K. An extension of the scattering theory beyond 150 *K*, not necessarily justified, predicts $E_{ph} = 109$ meV at 300 K. Density functional theory predicts a DoS with an energy range ≈ 3–107 meV, showing reasonable correlation with the QMC-derived E_{ph}. Support for the general applicability of our $\Delta\sigma$ vs d model, Eq. 3, comes from excellent fits to another material, GZO on fused silica. Finally, we considered an alternative model for the observation that very thin films can have a value of $\Delta\sigma$ above the maximum permitted by Kawabata's 3D theory. This alternative model suggested that the thinnest samples should be treated as 2D, not 3D. However, a direct comparison of 3D and 2D theories showed that the latter gave poor fits to all samples and thus could not explain the observed phenomena.

Methods

Sample growth. Ten ITO films, of thicknesses 13, 26, 37, 62, 74, 109, 149, 217, 242, and 292 nm (measured by spectroscopic ellipsometry), were deposited in a Neocera (Neocera LLC, 10000 Virginia Manor Rd # 300, Beltsville, MD 20705 USA) Pioneer 180 pulsed laser deposition system with a KrF excimer laser (Coherent COMPex Pro 110, $\lambda = 248$ nm, 10 ns pulse duration). The chamber base pressure was 2.66×10^{-6} Pa and a deposition pressure of 1.3 Pa was utilized with a 5% O_2 /95% Ar gas mixture. Double-side-polished, 2-inch-diameter, fused-silica substrates were heated by a backside heater to 300 °C and rotated during deposition. The laser operated at a pulse frequency of 30 Hz and an energy density of 2.6 J cm^{-2} measured at the target, which was 50-mm in diameter, 6-mm thick, 99.99%-pure, and composed of 90-wt%-In_2O_3 and 10-wt%-SnO_2. The target-to-substrate distance was 50 mm with a 45° laser angle of incidence to the target. Although these samples were not measured by X-ray diffraction (XRD), previous ITO growths by PLD on Si, in the same apparatus and under nearly identical conditions, were studied by XRD and found to be polycrystalline, even down to 10-nm thickness[8]. Similarly, Kim et al.[18] grew ITO on plastic (PMMA) by RF sputtering at 70 °C and found amorphous growth for $d < 80$ nm but polycrystalline growth for thicker samples, with dominant orientations of (222), (400), (440), and (622).

Hall effect, QMC. Hall effect and conductivity measurements were carried out in a LakeShore (LakeShore Cryotronics, Inc., 575 McCorkle Blvd, Westerville, OH 43082 USA) 7500 system over a temperature range $T = 10$–320 K, and at magnetic-field strengths $B = 0$ and 1 tesla. At each value of T, the automated system produced values of mobility $\mu(T)$, carrier concentration $n(T)$, and resistivities $\rho 0(T)$ (at $B = 0$), and $\rho B(T)$ (at $B = 1$ tesla). The experimental values of $\Delta\sigma(B,T)$ were calculated from $\Delta\sigma(B,T) = \rho B(T)^{-1} - \rho 0(T)^{-1}$, and the experimental values of $\mu_{tot}(T)$ and $n(T)$ were given directly by the apparatus. Thus, by fitting the experimental $\Delta\sigma\,(B,T)$ to the theoretical expression in Eqs. 1 and 2, the term $\mu_{ph}(T)$ in Eq. 2 is the only unknown and was determined by solving Eq. 1 as a transcendental equation.

Effective phonon energy calculation. The conversion of $\mu_{ph}(T)$ to an effective energy $kT_{ph}(T)$, representing all of the phonons responsible for the inelastic scattering at that temperature, was accomplished by solving Eq. 4 as a transcendental equation. This equation has been published elsewhere[9] and is a somewhat modified version of a first-order variational calculation due to Howarth and Sondheimer[19]. For In_2O_3, we use the values $\varepsilon_0 = 9.0$, $\varepsilon_\infty = 4.0$, and $m^* = 0.30m_0$[20]. Because Eq. 4 is only an approximation, we present $kT_{ph}(T)$ also as an approximation, and a more accurate analysis will require additional scattering theory. Nevertheless, the continuous dependence of the effective phonon energy has been interpreted as a mixing between the polar optical modes and nonscattering modes due to the large number of disordered donor sites[21]. The latter produce a particularly strong phonon mixing effect in complex oxides like β-Ga_2O_3 and $ZnGa_2O_4$, which have many, closely-spaced phonon branches[13]. A similar effect is found here for ITO by first-principles calculations, which show an interplay of mixing from Sn sites, In vacancies, and ITO polymorphism[21].

Density functional theory. The total phonon density of states was calculated for the perfect crystal, ignoring disorder from all causes. For that we used the Quantum Espresso software package[22], which included DFT for lattice structure, and density functional perturbation theory[23] for lattice dynamical properties (DFPT). We used ultrasoft pseudopotentials with the PBEsol exchange-correlation potential[24], a

plane-wave cut-off of 125 Ry, and a $16 \times 16 \times 8$ Monkhorst-Pack **k**-point grid for structure relaxation with a convergence criterion of 1 mRy/a.u. The Brillouin Zone sampling for lattice dynamical properties consisted of an $8 \times 8 \times 8$ **k**-point grid for the electrons and a $4 \times 4 \times 4$ **q**-point grid for phonons.

Data availability

The datasets generated during and/or analysed during the current study are available from the corresponding author on reasonable request.

Received: 25 September 2020; Accepted: 22 February 2021;
Published online: 23 March 2021

References

1. Mott, N. F. & Davis, E. A. *Electronic Processes in Non-Crystalline Materials* (Oxford University Press, 1971).
2. Lee, P. A. & Ramakrishnan, T. V. Disordered electronic systems. *Rev. Modern Phys.* **57**, 287–337 (1985).
3. Dugdale, J. S. *The Electrical Properties of Disordered Metals* (Cambridge University Press, 2005).
4. Kawabata, A. Theory of negative magnetoresistance in three-dimensional systems. *Solid State Commun.* **34**, 431–432 (1980).
5. Minami, T. Transparent conducting oxide semiconductors for transparent electrodes. *Semicond. Sci. Technol.* **20**, S35–S44 (2005).
6. Look, D. C. et al. Model for thickness dependence of mobility and concentration in highly conductive zinc oxide. *Opt. Eng.* **52**, 033801 (2013).
7. Itagaki, N. et al. Highly conducting and very thin ZnO:Al films with ZnO buffer layer fabricated by solid phase crystallization from amorphous phase. *Appl. Phys. Exp* **4**, 011101 (2011).
8. Cleary, J. W., Smith, E. M., Leedy, K. D., Grzybowski, G. & Guo, J. Optical and electrical properties of ultra-thin indium tin oxide nanofilms on silicon for infrared photonics. *Opt. Mater. Express* **8**, 1231–1245 (2018).
9. Look, D. C. & Leedy, K. D. Classical and quantum conductivity in β-Ga_2O_3. *Sci. Rep.* **9**, 1290 (2019).
10. Look, D. C. *Electrical Characterization of GaAs Materials and Devices* (Wiley, 1989).
11. Look, D. C., Leedy, K. D., Horng, Ray-Hua, Santia, M. D. & Badescu, S. C. Electrical and optical properties of degenerate and semi-insulating $ZnGa_2O_4$: electron/phonon scattering elucidated by quantum magnetoconductivity. *Appl. Phys. Lett.* **116**, 252104 (2020).
12. Hikami, S., Larkin, A. I. & Nagaoka, Y. Spin-orbit interaction and magnetoresistance in the two dimensional system. *Prog. Theor. Phys.* **63**, 707 (1980).
13. Santia, M. D., Look, D. C. & Badescu, S. C. Electron-phonon coupling and electron mobility in degenerately doped oxides from first principles. *Opt. Eng.* **59**, 067103 (2020).
14. Ma, N. et al. Intrinsic electron mobility limits in β-Ga_2O_3. *Appl. Phys. Lett.* **109**, 212101 (2016).
15. Ghosh, K. & Singisetti, U. Ab initio calculation of electron-phonon coupling in monoclinic β-Ga_2O_3 crystal. *Appl. Phys. Lett.* **109**, 072102 (2016).
16. Kang, Y., Krishnaswamy, Y. K., Peelaers, H. & Van de Walle, C. G. Fundamental limits on the electron mobility of β-Ga_2O_3. *J. Phys. Condens. Matter* **29**, 234001 (2017).
17. Chatratin, I. et al. Role of point defects in the electrical and optical properties of In_2O_3. *Phys. Rev. Mat.* **3**, 074604 (2019).
18. Kim, D. H., Park, M. R., Lee, H. J. & Lee, G. H. Thickness dependence of electrical properties of ITO film deposited on a plastic substrate by RF magnetron sputtering. *Appl. Surf. Sci.* **253**, 409–411 (2006).
19. Howarth, D. J. & Sondheimer, E. H. The theory of electronic conduction in polar semiconductors. *Proc. R. Soc. A* **219**, 53–74 (1953).
20. Preissler, N., Bierwagen, O., Ramu, A. & Speck, J. S. Electrical transport, electrothermal transport, and effective electron mass in single-crystalline In_2O_3 films. *Phys. Rev. B* **88**, 085305 (2013).
21. Karazhanov, S. Z. et al. Phase stability, electronic structure, and optical properties of indium oxide polytypes. *Phys. Rev. B* **76**, 075129 (2007).
22. Gianozzi, P. et al. Quantum ESPRESSO: a modular and open-source software project for quantum simulations of materials. *J. Phys. Condens. Matter* **21**, 395502 (2009).
23. Baroni, S., de Gironcoli, S., Dal Corso, A. & Giannozzi, P. Phonons and related crystal properties from density-functional perturbation theory. *Rev. Mod. Phys.* **73**, 515 (2001).
24. Perdew, J. P. et al. Restoring the density-gradient expansion for exchange in solids and surfaces. *Phys. Rev. Lett.* **100**, 136406 (2008).

Acknowledgements

This material is based upon work supported in part by the Air Force Office of Scientific Research under award number FA9550-RY18COR800. Further financial support was provided by the Air Force Research Laboratory under Contract FA8075-14-D-0025 and the National Science Foundation under grant DMR-1800139 (T. Paskova). We wish to thank T.A Cooper, W. Rice, and D. McFarland, for critical technical support in these experiments.

Author contributions

D.C.L. conceived of the project and carried out the Hall effect and magnetoconductivity modeling and calculations. K.D.L. developed the degenerate crystal growth methodology and performed the spectroscopic ellipsometry. M.D.S. and S.C.B. carried out the density functional calculations of phonon states including some aspects of disorder. All authors participated in writing the manuscript.

Competing interests

The authors declare no competing interests.

Additional information

Correspondence and requests for materials should be addressed to D.C.L.

Peer review information Primary handling editor: Aldo Isidori

Reprints and permission information is available at http://www.nature.com/reprints

Publisher's note Springer Nature remains neutral with regard to jurisdictional claims in published maps and institutional affiliations.